Received: 1 September 2018 | Revised: 18 August 2020 | Accepted: 20 November 2020

DOI: 10.1002/rnc.5355

SHORT COMMUNICATION

WILEY

Robust semiactive control of a half-car vehicle suspension system with magnetorheological dampers: Quantitative feedback theory approach with dynamic decoupler

Ramamurthy Jeyasenthil[1] | **Dal-Seong Yoon**[2] | **Seung-Bok Choi**[2] | **Gi-Woo Kim**[2]

[1]Electrical Engineering Department, National Institute of Technology, Warangal, Telangana, 506004, India

[2]Smart Structures and System Laboratory, Mechanical Engineering Department, Inha University, Incheon, South Korea

Correspondence
Seung-Bok Choi, Smart Structures and System Laboratory, Mechanical Engineering Department, Inha University, Incheon 402751, South Korea.
Email: seungbok@inha.ac.kr

Funding information
National Research Foundation of Korea (NRF), Grant/Award Number: 2017R1A2B3003026

Abstract

This article presents the quantitative feedback theory (QFT) based multivariable controller for the vertical and the pitch angle motion of a half-car suspension system. A coupled half-car system with significant uncertainty, due to sprung masses variation, poses a challenging control problem. Multi-input multi-output (MIMO) QFT method is used for this purpose which involves converting the actual MIMO system into an equivalent single-input single-output (SISO) system so that the design problem is carried out using the SISO QFT principles. The proposed idea is centered on by converting the coupled MIMO system into a decoupled one using the dynamic decoupler where in controllers are designed independently based on the equivalent SISO system. The designed QFT-based controllers with the decoupler use the semiactive suspension strategy (realized using the magnetorheological (MR) damper) to reduce the vibration of the half-car suspension system (in vertical/pitch angular motion) and hence to increase the ride comfort and the vehicle road holding. The feedback cost is *less* in the proposed design than the sequential QFT design. In this study, the MR damper dynamics is captured by the first-order model which is realistic, efficient, and simple form. Extensive comparative simulation studies are carried out to illustrate the effectiveness of the proposed design over the existing methods such as passive and skyhook control under different road excitation.

KEYWORDS

dynamic decoupler, half-car system, magnetorheological fluid, MR damper, quantitative feedback theory, robust control, semiactive suspension control, uncertain systems, vibration attenuation

1 | INTRODUCTION

The design of a vehicle suspension control system is an important task and has drawn considerable attention for significantly improving passenger comfort, safety, and vehicle maneuverability. From the perspective of the control system design, the vehicle suspension system can be classified as passive, active, and semiactive suspension.[1,2] Attenuating the harmful effects of the vibrations from various road conditions is the primary objective of any type of the suspension system. To achieve this, the designer has to make a compromise between the road holding and ride comfort requirements which is a conflicting one. Passive suspension is often inadequate to make this compromise in order to improve the performances.[2]

Active suspension can achieve better performances than passive and semiactive with the expense of high energy which restricts its use for production vehicles.[1-5] On the other hand, semiactive suspension deliver the forces which can vary with respect to the relative motion of the suspension velocity to improve the performance.[6,7] And it works without any extra-large power sources and expensive hardware as in the case of active suspension. This makes the semiactive control a suitable choice for the industry to adapt it to control the vehicle suspension system as it combines the advantage of both passive and active suspension system.

The semiactive suspension has been applied over many of practical systems such as road vehicle suspension, seat suspension, lateral suspensions in high speed trains, landing gears in aircraft, suspensions of appliances (such as washing machines), architectural suspensions (building, bridges), cabin engine mount system.[8] This work focuses on road vehicle suspension. In this work, semiactive control of half-car suspension system employed with magnetorheological (MR) dampers is considered. MR damper-based semiactive suspension system has attracted the researcher's attention due to its benefits such as fast response time, low energy consumption, and compact size. And some passenger vehicles with MR damper suspension are running on the road in practice. A large number of control methodologies exist for the semiactive suspension control. Among them, the most famous one is the skyhook (SH) control strategy.[9] The main source of the uncertainty in the half-car system is the payload (or) no of the passenger which inturn changes the vehicle moment of inertia. The uncertainty present in the system invites the robust control techniques into the picture to effectively control the suspension system.

Robust control design methods for the semiactive suspension control system are reported in the literature. For instance, H_∞ controller is designed for the quarter car system with electrorheological damper being modeled as a first-order system in Reference 6. The MR damper dynamics is modeled using the polynomial method[10] and controlled using the static output feedback H_∞ controller in Reference 7. Linear parameter varying (LPV) technique-based semiactive system is introduced in Reference 11 with the help of H_∞ control. Apart from the suspension control of the quarter car system, a number of semiactive control techniques have been investigated for the half-car system. For example, a linear quadratic Gaussian-based semiactive control is proposed in Reference 12 with the MR dampers as the actuators. In Reference 13, H_∞ control with/without preview control-based semiactive control system is adapted to meet the performance comparable to that of the active suspension control. Furthermore, the same authors explored the application of the linear quadratic regulator with full state and limited state feedback in Reference 14. A novel dual MR dampers-based controllable suspension system for half-car model is proposed in Reference 15. Recently, LPV-based feedforward control of semiactive suspensions for the half-car system is proposed in Reference 16 to improve the roll stability. In this work, we mainly focus on the development of robust control method known as quantitative feedback theory (QFT) for the half-car suspension system.

The application of QFT to vehicle suspension system is concerned, very few works are available in the literature. To name them, the cascade QFT design proposed in Reference 17 and the comparative study between the H_∞ and QFT control in Reference 18. However, these were applied to the active suspension system. For semiactive suspension, the work reported in Reference 19 is the first application of QFT. Recently, the authors proposed a QFT-based novel semiactive suspension control in Reference 20 to address the problems such as MR damper fault and saturation, and the damping force tracking problem using the cascade approach in Reference 21. Moreover, so far, the application of QFT to vehicle suspension control is restricted to the quarter car suspension system. This motivates us to expand the application of QFT to the challenging multivariable half-car suspension control system.[22]

The challenges and technical contributions associated with this specific control problem are summarized as follows:

1. An independent single-input single-output (SISO) QFT method with a dynamic decoupler is proposed for the semiactive control of the half-car suspension system.
2. The presence of the coupling in the multi-input multi-output (MIMO) half-car system poses a challenging control problem. The dynamic decoupler is introduced to reduce the coupling effects in the half-car system and the resultant system becomes the diagonally dominant one (decoupled). That is, the coupled MIMO system is converted into the decoupled MIMO system which is diagonally dominant one.
3. The SISO QFT principle is applied on the diagonally dominant system (equivalent SISO systems) to control the vertical and the angular pitch motion of the chassis. To the best of author's knowledge, this work is the *first* of its kind where in QFT (with decoupler) being applied to control (semiactive) the half-car suspension system featuring MR dampers.
4. The proposed design results in the *less feedback cost* (in QFT terms) as compared with the existing sequential design. The effectiveness of the proposed approach is compared with the skyhook and passive control. It is found to deliver better performance (ride comfort, road holding) in terms of acceleration, tyre deflection under different road excitations.

The proposed approach achieves the smaller peak values in the power spectral density (PSD) of vertical and the pitch angle accelerations (around 1–2 Hz) as compared with the skyhook control and passive.

The remainder of this article is organized as follows. We start with some background material related to the MR damper and the half-car suspension model in Section 2. The proposed approach consists of the decoupler and the feedback controller design is discussed in Section 3. The relative gain array (RGA) analysis followed by the synthesis of the decoupler and the controllers are carried out in Section 4. Next, the performance analysis of the proposed design is compared over the existing methods under different road excitation in Section 5. Finally, the outcome of the case study is drawn as a conclusion in Section 6.

2 | BACKGROUND

2.1 | MR damper dynamics

The application of MR damper to the semiactive suspension control system significantly depends on the modeling of the MR dampers which is inherently hysteretic and nonlinear dynamics. The simple way to describe the behavior of MR damper is by using the first-order dynamics.[6,22] Even if some nonlinear effects are neglected, this model is a realistic approximation of the actual MR damper. The actual damping force (F_i) of the i^{th} MR damper can be modeled as first-order system given by

$$\tau_i \dot{F}_i + F_i = u_i, \tag{1}$$

where, τ_i is the time constant of the i^{th} MR damper ($i = 1,2$) and u_i is the desired damping force from the controller.

2.2 | Half-car model

In this work, a half-car with MR suspension system is used to evaluate the performance and robustness of the control system. A half-car model with an MR damper is shown in Figure 1. The dynamics of the half-car suspension system are given as follows[12]

$$\begin{aligned}\ddot{z_c} = {} & \frac{-(k_1+k_2)}{M} z_c - \frac{(k_1 b_1 - k_2 b_2)}{M}\phi + \frac{k_1}{M} z_{t1} + \frac{k_2}{M} z_{t2} - \frac{(c_1+c_2)}{M}\dot{z_c} - \frac{(c_1 b_1 - c_2 b_2)}{M}\dot{\phi} + \frac{c_1}{M}\dot{z_{t1}} \\ & + \ldots \frac{c_2}{M}\dot{z_{t2}} + \frac{F_1}{M} + \frac{F_2}{M}\end{aligned} \tag{2}$$

$$\begin{aligned}\ddot{\phi} = {} & \frac{-(k_1 b_1 - k_2 b_2)}{I} z_c - \frac{(k_1 b_1^2 - k_2 b_2^2)}{I}\phi - \frac{k_1 b_1}{I} z_{t1} + \frac{k_2 b_2}{I} z_{t2} - \frac{(c_1 b_1 - c_2 b_2)}{I}\dot{z_c} - \frac{(c_1 b_1^2 + c_2 b_2^2)}{I}\dot{\phi} \\ & - \ldots \frac{c_1 b_1}{I}\dot{z_{t1}} + \frac{c_2 b_2}{I}\dot{z_{t2}} + \frac{b_1}{I} F_1 - \frac{b_2}{I} F_2\end{aligned} \tag{3}$$

$$\ddot{z_{t1}} = \frac{k_1}{m_{t1}} z_c + \frac{k_1 b_1}{m_{t1}}\phi - \frac{(k_1 + k_{t1})}{m_{t1}} z_{t1} + \frac{c_1}{m_{t1}}\dot{z_c} + \frac{c_1 b_1}{m_{t1}}\dot{\phi} - \frac{(c_1 + c_{t1})}{m_{t1}}\dot{z_{t1}} - \frac{1}{m_{t1}} F_1 + \frac{k_{t1}}{m_{t1}} z_{r1}, \tag{4}$$

$$\ddot{z_{t2}} = \frac{k_2}{m_{t2}} z_c - \frac{k_2 b_2}{m_{t2}}\phi - \frac{(k_2 + k_{t2})}{m_{t2}} z_{t2} + \frac{c_2}{m_{t2}}\dot{z_c} - \frac{c_2 b_2}{m_{t2}}\dot{\phi} - \frac{(c_2 + c_{t2})}{m_{t2}}\dot{z_{t2}} + \frac{-1}{m_{t2}} F_2 + \frac{k_{t2}}{m_{t2}} z_{r2}. \tag{5}$$

Equations (2) and (3) describes the dynamics of the vertical (z_c) and pitch angle (ϕ) of the chassis. The unsprung mass (wheel assembly z_{t1}, z_{t2}) dynamics is described in Equations (4) and (5).

The state space model for the half-car MR suspension system, from Equations (1)–(5), is written by

$$\dot{x} = Ax + Bu + Lz_r \tag{6}$$

and the output equation is $y = Cx$.

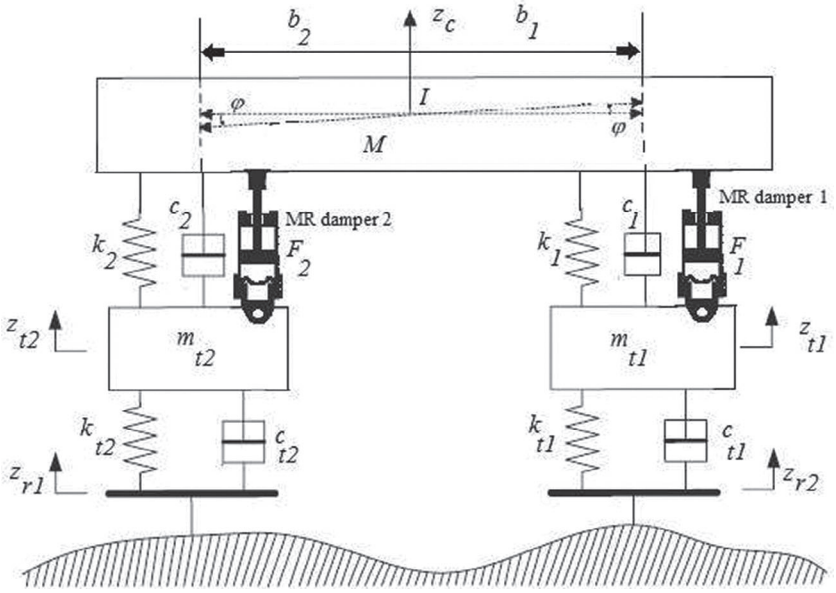

FIGURE 1 Half-car semiactive suspension model with the magnetorheological dampers

Here, $A \in \mathcal{R}^{10\times10}$, $B \in \mathcal{R}^{10\times2}$, $C \in \mathcal{R}^{2\times10}$, and $L \in \mathcal{R}^{10\times2}$ are the system matrix, the control input matrix, the output matrix and the disturbance matrix, respectively. These matrices are given in the appendix.

The state space variables are defined as $x = [z_c,\ \phi,\ z_{t1},\ z_{t2},\ \dot{z}_c,\ \dot{\phi},\ \dot{z}_{t1},\ \dot{z}_{t2},\ F_1,\ F_2]^T$. The sprung mass 1 and 2 are related to the vertical and the pitch angle motion of the chassis by the following relation[3]

$$z_{s1} = z_c - b_1\phi, \tag{7}$$

$$z_{s2} = z_c + b_2\phi. \tag{8}$$

In practice, the chassis mass (M) and the moment of inertia (I) are varied by the loading conditions such as the number of riding person and payload. The time constants (τ_1, τ_2) of the MR dampers is not easy to measure accurately as it depends on the operating temperature. So, this is also considered as an uncertain parameter, that is, Chassis mass $M \in [600,\ 800]$ kg, chassis inertia $I \in [1100,\ 1300]$ kgm^2, the time constant $(\tau_i) \in [0.018,\ 0.022]$ s. And the unsprung mass values of front (m_{t1}) and rear (m_{t2}) wheels are 45 and 40 kg; stiffness coefficient of front (k_1) and rear (k_2) are 24,000 and 20,000 N/m; tire stiffness coefficient of front (k_{t1}) and rear (k_{t2}) are 240,000 and 200,000 N/m; damping coefficient of front (c_1) and rear (c_2) are 600 and 600 Ns/m; tire damping coefficient of front (c_{t1}) and rear (c_{t2}) are 1000 and 900 Ns/m; distances b_1, b_2 are 1 and 1.4 m, respectively.

3 | PROPOSED APPROACH

The proposed approach involves the two main ingredients such as the decoupler design and then the feedback controller design. The rationale behind the introduction of the decoupler is to reduce the interaction effect on the actual output in the MIMO half-car system. After reducing the coupled dynamics of the MIMO system into a decoupled one, the SISO QFT method is employed to design the feedback controllers to control the sprung masses which in turn reduces the vibration in the vertical and the pitch angle motion, respectively.

3.1 | Decoupler design

The crosscoupling behavior of the half-car system needs to be minimized. There exist a couple of approaches to address the crosscoupling problem and some of them are the design of the diagonal controller and the nondiagonal controller matrix using the sequential QFT methods,[23] respectively. These methods increase the design complexities[24] and involve an overdesign in the first control loop. Therefore, an independent design approach with the dynamic decoupler is preferred.

The dynamic decoupler reduces the crosscoupling present in the actual system and converts it into a diagonally dominant MIMO system (noninteracting).

The plant transfer function matrix (TFM) for the (2×2) system is defined as

$$P(s)=\begin{bmatrix} p_{11}(s) & p_{12}(s) \\ p_{21}(s) & p_{22}(s) \end{bmatrix};\quad p_{ij}\in\mathcal{P};\quad i,\ j=1,2.$$

The dynamic decoupler[1] for the (2×2) system is given as follows[25]

$$D_e(s)=\begin{bmatrix} d_{e11}(s) & d_{e12}(s) \\ d_{e21}(s) & d_{e22}(s) \end{bmatrix}=\begin{bmatrix} 1 & \frac{-p_{120}(s)}{p_{110}(s)} \\ \frac{-p_{210}(s)}{p_{220}(s)} & 1 \end{bmatrix}. \tag{9}$$

3.2 | Independent SISO QFT method

We apply the independent SISO QFT method[23] to design the feedback controller for the decoupled system. The independent SISO method works on the system formulated using the on-diagonal element of the MIMO system. For the Half-car suspension system, this method suits more appropriately as the decoupler makes the actual coupled MIMO system into a decoupled one and then we apply the SISO QFT principles.

The closed loop output disturbance TFM S, which relates the output Y and the road excitation input Z_r, is denoted as follows:

$$[I+PG]S=I. \tag{10}$$

Here, the $(n\times n)$ plant transfer matrix is denoted as $P=[p_{ij}]\in\mathcal{P}$ with $i,\ j=1,2,\ \dots\ ,n$ and $G=\text{diag}[g_{ii}]$ represents the $(n\times n)$ diagonal controller matrix.

For the decoupled system, the closed loop disturbance TFM becomes

$$[I+P_eG]S=I. \tag{11}$$

Here, the plant transfer matrix with the decoupler is denoted as $P_e=D_eP$.

The objective is to design a diagonal feedback controller matrix G such that the closed loop is internally stable and the disturbance rejection specification given as follows satisfied.

$$|S(j\omega)|\le B_d(\omega). \tag{12}$$

In terms of elements, we can write the above as

$$|s_{ij}|\le b_{dij}; \tag{13}$$

where, $B_d=[b_{dij}]$ is the disturbance rejection tolerance matrix.

The QFT bounds are calculated based on the uncertain on-diagonal plant element $p_{ii}(s)$ from the MIMO system. The output disturbance rejection specification for the ith equivalent SISO loop[2] is given as

$$\left|\frac{1}{1+p_{eii}(j\omega)g_{ii}(j\omega)}\right|\le b_{dii}(\omega); \tag{14}$$

And the robust stability margin for the ith equivalent SISO loop is described as

$$\left|\frac{p_{eii}(j\omega)g_{ii}(j\omega)}{1+p_{eii}(j\omega)g_{ii}(j\omega)}\right|\le w_{sii}; \tag{15}$$

[1]The subscript "0" denotes the nominal plant element.
[2]The terms SISO loop-i and ith equivalent SISO loop are interchangeably used throughout the article.

Here, w_{sii} is the stability margin specification (i.e., M-circle magnitude corresponding to the desired gain and phase margin).

The proposed idea is based on the simplified decoupling combined with the independent SISO QFT design (non-sequential). The independent SISO QFT design is carried out on the decoupled plant (diagonal) element as opposed to the original plant element which has been the approach used in conjunction with the decoupler (remark 8.2 in Reference 23).

Remark 1. There exist many MIMO QFT methods in the literature such as the sequential design with the diagonal controllers and nondiagonal controllers.[26,27] As mentioned in Reference 24, these methods increase the complexity of design and decrease the accessibility of online calibration. Especially, the nondiagonal controller design is more involved for the full car suspension (4×4 system) control design. The design of decoupler element is not always an easy task as it is required to lie in the mean value of magnitude and phase of the Bode diagram of expression (8.176 in Reference 23-Method 2).

Remark 2. In Method 1, the simplified decoupling is used but its design is combined with the diagonal feedback controller (section 8.7 in Reference 23). As mentioned in section 8.7 of Reference 23, the design involved in Method 1 is somewhat complicated, that is, a redesign in any feedback controller leads to redesign of all the diagonal and off-diagonal elements of decoupler (subsequent loop). In other words, a decoupler element design is not independent of the feedback controller.

3.3 | Some existing methods

3.3.1 | Sequential QFT method

For comparison purpose, if required, we consider the sequential MIMO QFT design methods. In sequential design, the explicit knowledge of the interactions between the equivalent SISO loops is accounted using the equivalent plant element. That is, the concept of the equivalent plant takes into account the controllers that were designed in the previous loop while performing the design in the successive loops.[23]

The design equation for (2×2) system,[28] such as Half-car suspension, is given as

$$|y_1| = \left| \frac{\pi^1_{11} z_{r1} + \pi^1_{12} z_{r2} - \pi^1_{12} y_2}{\pi^1_{11} + g_{11}} \right| \leq b_{d11}(\omega); \tag{16}$$

$$|y_2| = \left| \frac{\pi^2_{21} z_{r1} + \pi^2_{22} z_{r2}}{\pi^1_{22} + g_{22}} \right| \leq b_{d22}(\omega). \tag{17}$$

Where, $P^{-1} = [\pi^1_{ij}]$; $i = j = 1, 2$. $\pi^2_{21} = \frac{\pi_{21} g_{11}}{\pi_{11} + g_{11}}$; $\pi^2_{22} = \pi_{22} - \frac{\pi_{21}\pi_{12}}{\pi_{11} + g_{11}}$;

The choice of loop selection in sequential design has the great influence on the design conservatism and its ability to meet the design specifications in the nonclosed loop.

3.3.2 | Skyhook control

The SH controller is the simplest control, but very effective in a semiactive control system associated with MR damper.[29] The approach is to virtually create an ideal suspension system in which the chassis is "hooked" to a virtual inertial frame called "sky" by a passive damper C_{sky}, then using the real suspension with a semiactive damper to create the dynamics of this ideal suspension system.[30] The control input of the SH controller (u) is defined as follows

$$u = C_{\text{sky}} z_s,$$

where C_{sky} is the control gain and z_s is the sprung mass position. The control gain is chosen by trial-and-error based on the magnitude of required damping force. It is the most widely used industrial control strategy which is easy to implement in the real field.[29]

4 | SYNTHESIS OF THE DECOUPLER AND THE FEEDBACK CONTROLLER

4.1 | RGA analysis

The crosscoupling effect (interaction) of the half-car system is quantitatively analyzed. For this purpose, the RGA is used to measure the interaction between the sprung mass 1 and 2 connected to the chassis. The RGA provides the comprehensive measurement for MIMO system behavior at steady state.[31] With the nominal values of M_0= 800 kg, $I_0 = 1275$ kgm^2, τ_i = 0.02 s for the half-car system, the RGA matrix was evaluated as follows

$$\text{RGA} = \begin{bmatrix} 0.5833 & 0.4167 \\ 0.4167 & 0.5833 \end{bmatrix}. \tag{18}$$

We observe that the gains of the off-diagonal elements are comparable to that of the on-diagonal elements. This implies that there exists considerable interaction between the sprung masses and inturn vertical and pitch angle motion. Here, the control loop represents the MR damper 1 and 2 controls the front sprung mass displacement (i.e., $F_1 \rightarrow z_{s1}$) and rear sprung mass displacement (i.e., $F_2 \rightarrow z_{s2}$), respectively.

A decoupler design is carried out on the nominal plant element of the uncertain plant TFM as discussed in Section 3.1. The elements of the decoupler TFM are given as

$$\frac{-p_{120}(s)}{p_{110}(s)} = \frac{-s^6 - 79.8s^5 - 1.142e04s^4 - 4.025e05s^3 - 2.606e07s^2 - 9.265e07s - 1.166e09}{s^6 + 74.74s^5 + 1.149e04s^4 + 3.982e05s^3 + 2.679e07s^2 + 1.049e08s + 1.645e09}, \tag{19}$$

$$\frac{-p_{210}(s)}{p_{220}(s)} = \frac{0.8667s^6 + 112.1s^5 + 1.282e04s^4 + 6.099e05s^3 + 2.68e07s^2 + 7.77e07s + 1.218e09}{s^6 + 123.9s^5 + 1.48e04s^4 + 6.93e05s^3 + 3.112e07s^2 + 7.92e07s + 9.975e08}. \tag{20}$$

The decoupled nominal system is denoted as $P_{e0} = P_0 D_e$. And, the RGA matrix of the P_{e0} becomes

$$\text{RGA} = \begin{bmatrix} 1 & 0 \\ 0 & 1 \end{bmatrix}. \tag{21}$$

The noninteracting behavior after applying the decoupler is only guaranteed for the nominal plant, and has only been checked quantitatively for steady state. None other specific quantitative verification on interaction has been performed for other frequencies or uncertain plants out of the nominal values, so that a general reference to the achievement of noninteraction can be made. Indeed, this might be the main drawback of the application of the proposed methodology to some systems: the resulting "decoupled system" out of the nominal behavior could still present relevant interaction not to be ignored by direct application of SISO design over the equivalent plant P_e.

The off-diagonal elements of the RGA matrix are zero and it shows that the noninteracting behavior of the MIMO system with the designed decoupler. Now, the independent SISO QFT design method (discussed in Section 3.2) is applied to the resulting system in the forthcoming section.

Remark 3. For the system with time delay, the static decoupler is preferred over the dynamic decoupler (due to instability problem).

4.2 | Feedback controller design

The MIMO control structure with the decoupler for the half-car system and its equivalent SISO loops are shown in Figure 2. The diagonal feedback controller $G = \text{diag}(g_{11}, g_{22})$ is designed using the independent SISO QFT method. For this, the desired specifications for both SISO loops are given as:

- Robust output sensitivity problem: $S = s_{ij} = (I + P_e G)^{-1}$;

$$|s_{ij}(j\omega)| \leq b_{dij}(\omega);$$

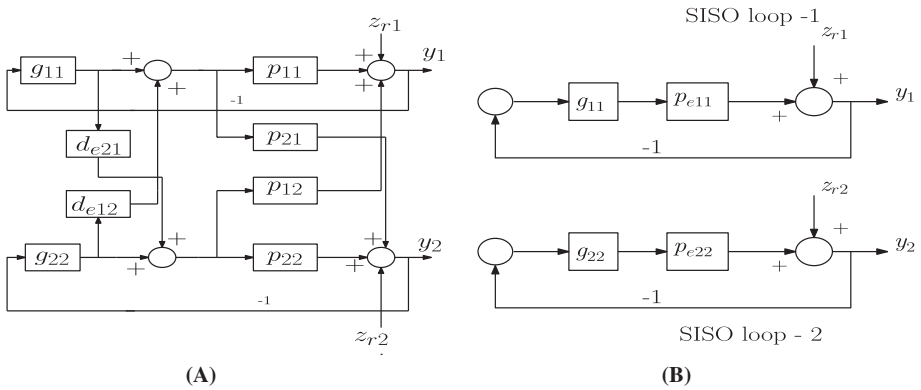

FIGURE 2 Control structure for the half-car system; (A) decentralized MIMO with the dynamic decoupler and (B) an equivalent SISO loops. MIMO, multi-input multi-output; SISO, single-input single-output

TABLE 1 Comparison of the bound values between the sequential QFT[28] and the proposed QFT method

	Sequential QFT[28] (dB)		Proposed method (dB)		Difference in bound values (dB)	
Frequency (rad/s)	**Minimum**	**Maximum**	**Minimum**	**Maximum**	**Minimum**	**Maximum**
1 (Loop-1)	30.5	31.5	12.25	15.75	**18.25**	**15.75**
1.5	23.5	24.6	7.75	13.8	**15.75**	**10.8**
2.5	15.6	18.05	9.87	0.97	**5.73**	**17.08**
5	3.4	11.75	−13.5	6.9	**16.9**	**4.85**
1 (Loop-2)	25.17	26.1	6.2	12.1	**18.97**	**14**
1.5	17.6	19.6	0.41	9.75	**17.19**	**9.85**
2.5	6.8	12.5	−11.6	7.125	**−18.4**	**5.37**

Abbreviation: QFT, quantitative feedback theory.
Note: The bold values indicate the difference between the existing methods and the proposed design.

where the disturbance rejection tolerance is

$$b_{d11}(\omega) = \left|\frac{1.5s}{s+1.2}\right|_{s=j\omega}; \tag{22}$$

$$b_{d22}(\omega) = \left|\frac{2.5s}{s+1.2}\right|_{s=j\omega}; \tag{23}$$

$$b_{dij} = 0; \quad i \neq j.$$

- Robust stability margins: Gain margin ≥ 5.5 dB, Phase margin ≥60° and its corresponding M- circle magnitude is around 2.5.

$$\left|\frac{p_{eii}(j\omega)g_{ii}(j\omega)}{1+p_{eii}(j\omega)g_{ii}(j\omega)}\right| \leq 2.5; \quad i = 1, 2. \tag{24}$$

The design frequency set Ω =[1,1.5,2.5,5,7.5,10 12 20 25 30 40 50 60 150 180] rad/s. To begin with, the comparison of the performance bounds generated using the sequential QFT[28] and the proposed method is shown in Figure 3 for both SISO loops. The proposed method (represented by B) requires less gain to satisfy the bounds than the sequential method bounds (denoted as SB) for both loops. As observed in Table 1, the proposed method bounds are better than the sequential one. For instance, the difference between the proposed and the sequential method bound value (maximum) is around 15 dB at $\omega = 1$ for SISO loop-1. Similarly, for SISO loop-2, this difference is around 14 dB. This illustrates that the proposed method for both the loops requires much less controller gain than the existing sequential QFT design.

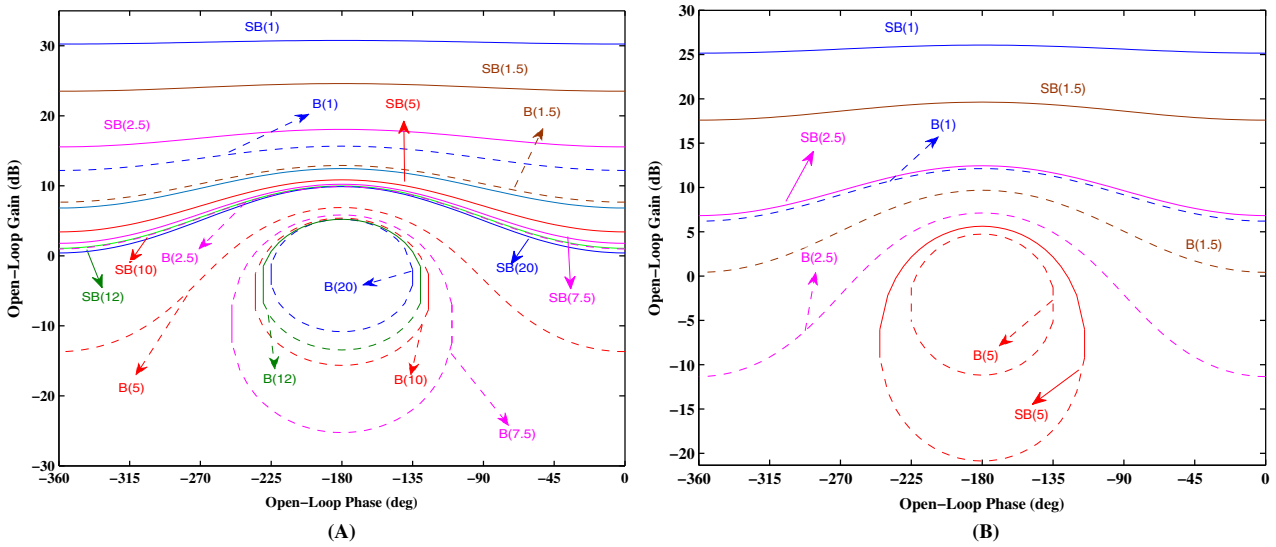

FIGURE 3 Comparison of the performance bounds generated using the proposed method (denoted as "B") and the sequential method (represented by "SB") at each performance design frequency; (A) SISO Loop-1 and (B) SISO Loop-2. SISO, single-input single-output [Colour figure can be viewed at wileyonlinelibrary.com]

4.3 | SISO loop-1 (Front sprung mass)

The feedback controller g_{11} design for SISO loop-1 is carried out using the proposed method in this section. For this purpose, the closed loop specifications (22,24) are translated into a set of bounds on the nominal loop transmission function (l_{110}) at each design frequency. The feedback controller g_{11} is designed such that the l_{110} lies on or above the open bounds and outside the closed bounds as shown in Figure 4(A). And the designed controller is

$$g_{11}(s) = \frac{19{,}537\left(\frac{s^2}{2^2} + \frac{2\times 0.85 s}{2} + 1\right)}{s\left(\frac{s^2}{60^2} + \frac{2\times 0.85 s}{60} + 1\right)}. \tag{25}$$

4.4 | SISO loop-2 (Rear sprung mass)

Next step in the proposed method is to design the feedback controller g_{22} for the equivalent SISO loop-2. As shown in Figure 4(B), the nominal loop transmission function l_{220} is shaped such that it respects the open performance bounds and the closed stability margin bounds at each design frequency. The designed controller g_{22} for the SISO loop-2 is

$$g_{22}(s) = \frac{-16{,}206\left(\frac{s^2}{2.5^2} + \frac{2\times 0.5 s}{2.5} + 1\right)}{s\left(\frac{s^2}{50^2} + \frac{2\times 0.95 s}{50} + 1\right)}. \tag{26}$$

The frequency domain analysis of the proposed design (both the loops) for the disturbance rejection specification is shown in Figure 5. The magnitudes (worst case) of the closed loop frequency response of the system satisfies the tolerance limits (22-23) for both the loops.

4.5 | Controller magnitude response comparison

The feedback controller design using the existing sequential QFT design is also carried out for comparison purpose.[23,28] The designed controllers for both SISO loops are denoted as Sg_{11} and Sg_{22}, respectively and given in Table 2. The

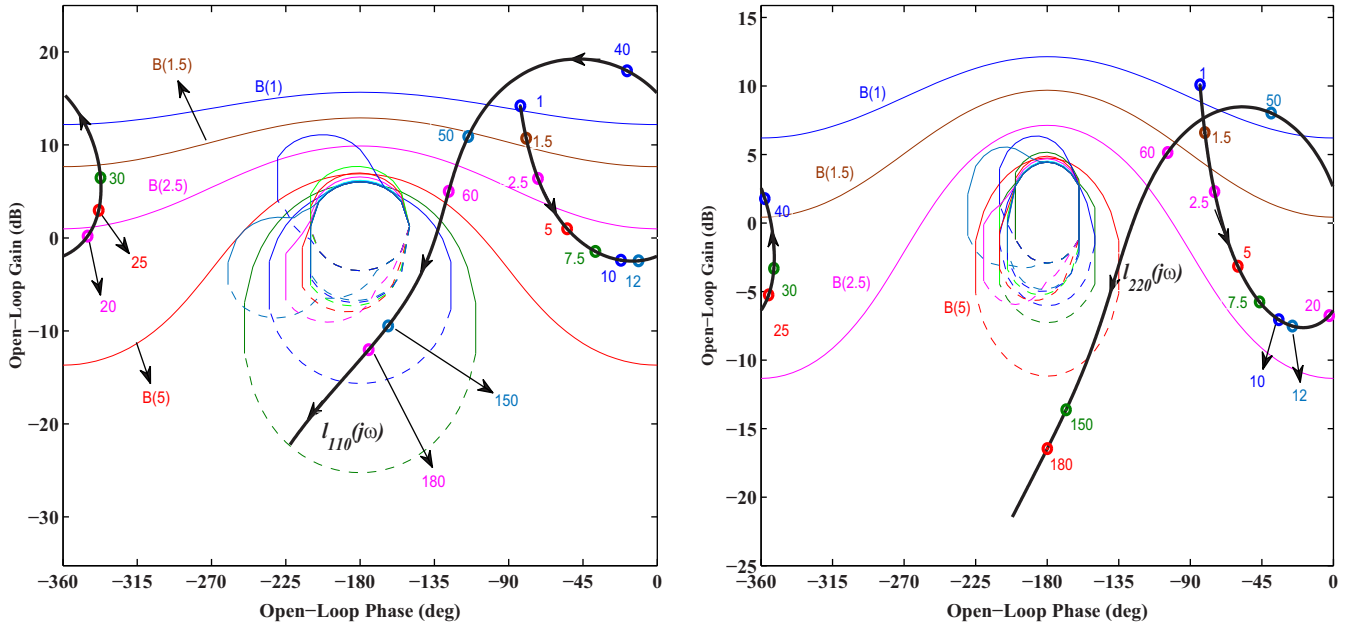

FIGURE 4 Nominal loop shaping plots for (A) SISO loop-1 and (B) SISO loop-2. Here, B(ω) represents the bounds generated using the proposed method at each performance design frequency. SISO, single-input single-output [Colour figure can be viewed at wileyonlinelibrary.com]

FIGURE 5 Frequency domain validation of the proposed design (worst case) for both the loops [Colour figure can be viewed at wileyonlinelibrary.com]

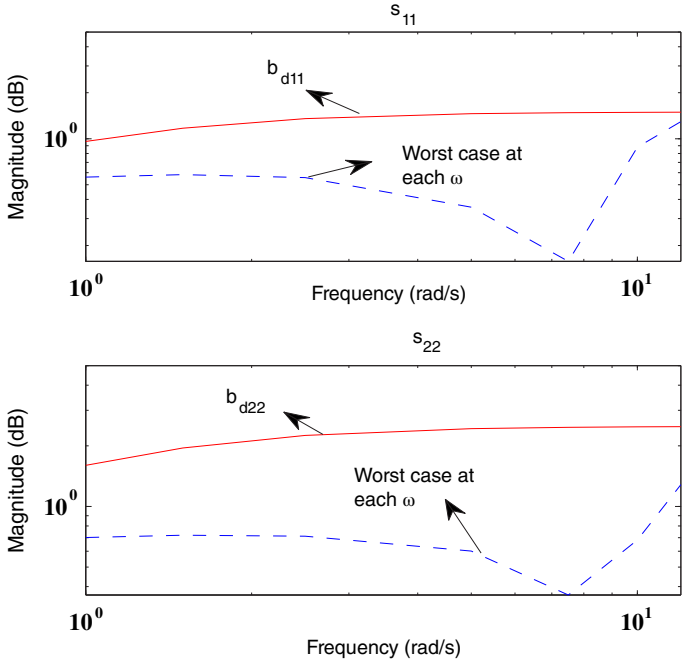

loopshaping plots for the sequential QFT design are omitted for simplicity. Figure 6 compares the controllers frequency response magnitude of the proposed design and the sequential design. The proposed design achieved the high-frequency (HF) gain reduction of around 10 and 15 dB over the sequential design for SISO loop 1 and 2, respectively. This implies that the proposed controllers have low bandwidth and the closed loop system employed with the proposed design is least sensitive to noise amplification as compared with the existing sequential method. Hereafter, we consider the proposed design for the performance analysis stage and drop the sequential design for further analysis due to its conservative design.

Method	Feedback controllers	
	Loop-1	Loop-2
Sequential method[28]	$Sg_{11}(s) = \frac{130{,}081(0.65{,}3.84)}{s(0.55{,}90)}$	$Sg_{22}(s) = \frac{-104{,}876.4(0.95{,}4.454)}{s(0.47{,}90)}$
Proposed method	$g_{11}(s) = \frac{19{,}537(0.85{,}2)}{s(0.85{,}60)}$	$g_{22}(s) = \frac{-16{,}206(0.5{,}2.5)}{s(0.95{,}50)}$

TABLE 2 Controllers designed using the existing sequential QFT method and the proposed method for both SISO loops

Note: Here, the notation (b, c) for $\left(\frac{s^2}{b^2} + \frac{2cs}{b} + 1\right)$ is used.

Abbreviations: QFT, quantitative feedback theory; SISO, single-input single-output.

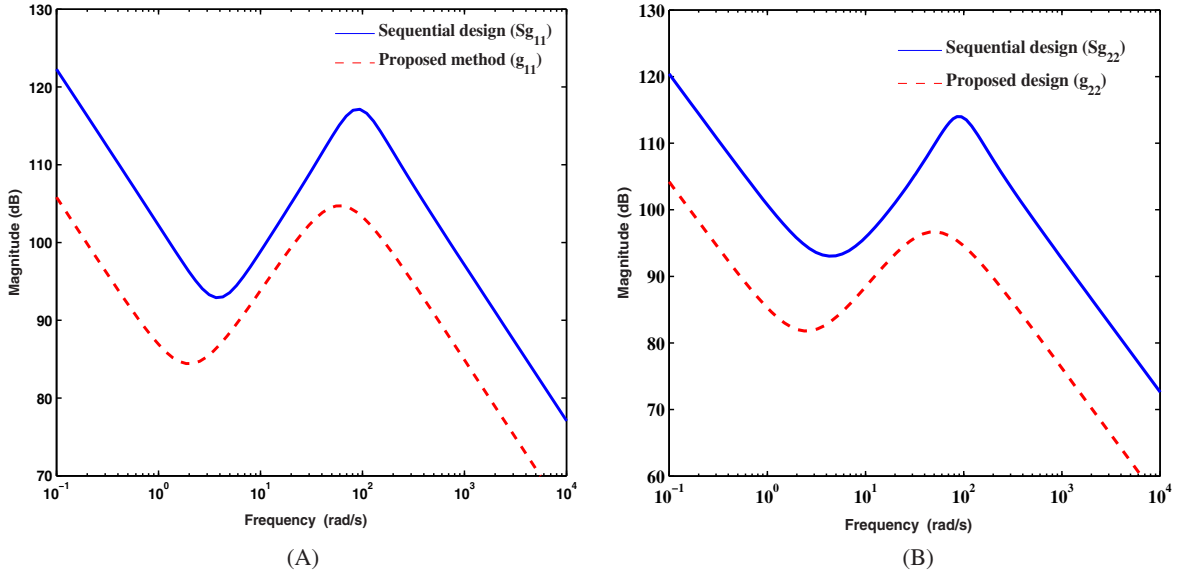

FIGURE 6 Comparison of controller magnitudes (Table 2) using the proposed method and the sequential method;[28] (A) SISO Loop-1 and (B) SISO Loop-2. SISO, single-input single-output [Colour figure can be viewed at wileyonlinelibrary.com]

5 | PERFORMANCE ANALYSIS

The performance of the proposed design for the half-car suspension control system is evaluated under three types of road excitation, that is, bump, sine, and random excitations. Hereafter, the *proposed design* denotes the decoupler given in Equations (19)–(20) and the feedback controller in (25)–(26). The most widely used industrial SH controller (discussed in Section 3.3) is considered for the comparison purpose with the following semiactuation condition:

$$U_i = \begin{cases} u_i, & (\dot{z}_{si} - \dot{z}_{ui}) > 0; \quad i = 1, 2. \\ 0, & (\dot{z}_{si} - \dot{z}_{ui}) \leq 0. \end{cases} \tag{27}$$

Here, the desired damping force of the ith damper is set as $u_i = C_{\text{sky}}\dot{z}_{si}$ and the control gain C_{sky} is chosen as 9000 for both dampers.

5.1 | Bump disturbance

The following bump excitation has been widely used to study the transient response characteristic[20] and is described by

$$z_{r1} = \frac{h}{2}(1 - \cos(\omega_r t)); \quad 0.1 < t < 0.75; \tag{28}$$

$$z_{r2} = \frac{h}{2}(1 - \cos(\omega_r t)); \quad 1 < t < 1.75; \tag{29}$$

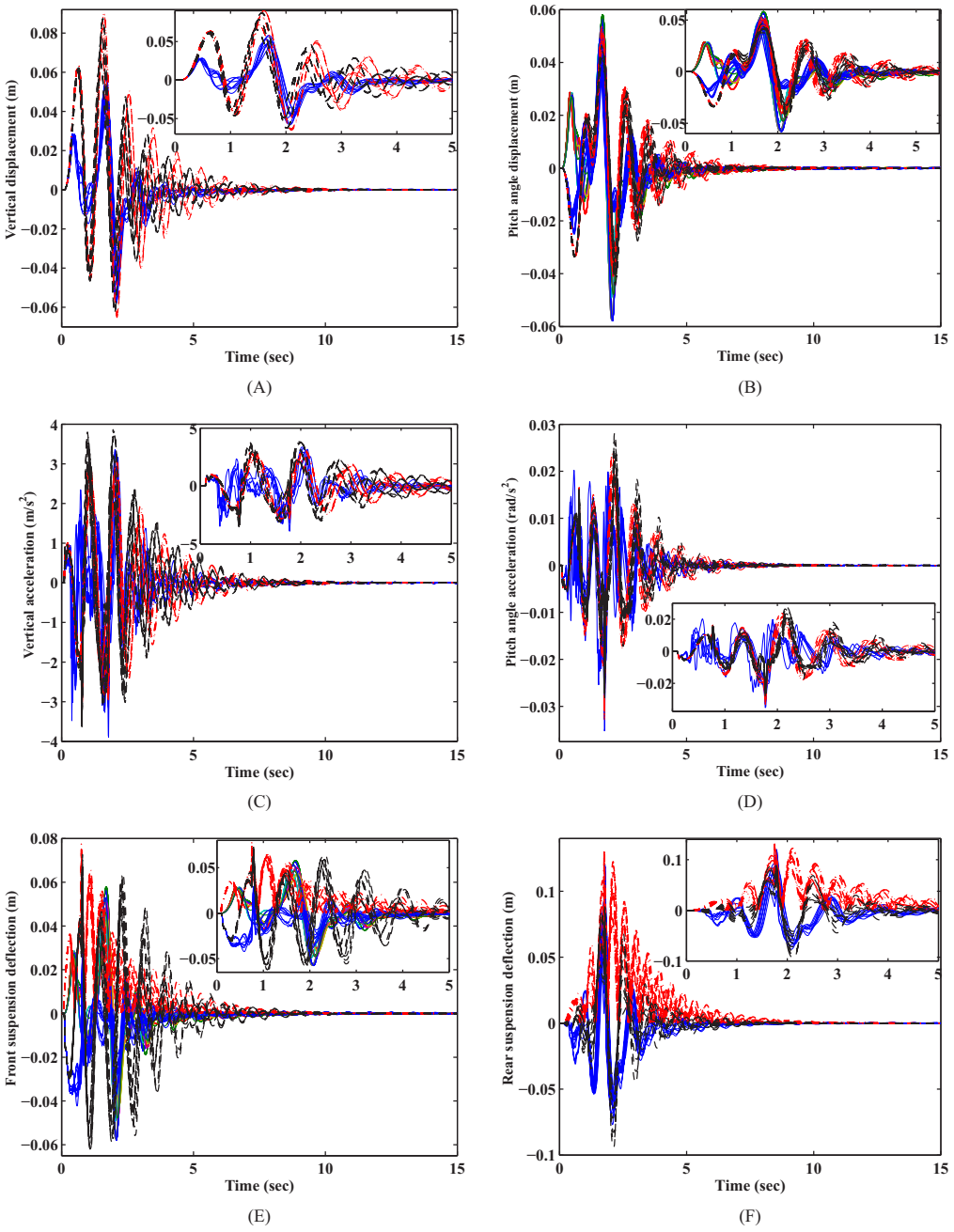

FIGURE 7 Bump responses for the (A) vertical displacement, (B) pitch angle displacement, (C) vertical acceleration, (D) angular acceleration, (E) front suspension deflection, and (F) rear suspension deflection. The responses denoted by dash-dot red line, dashed black line, and blue line represents the passive control, Sky hook, and the proposed control, respectively [Colour figure can be viewed at wileyonlinelibrary.com]

where, $h = 0.03$ m is the bump height, and $\omega_r = 2\pi V/D$, the width of the bump (D) is 0.8 m. And, the vehicle travels the bump with constant velocity (V) of 0.833 m/s. If the vehicle velocity increases, damper will reach the stopper mode due to maximum stroke increased as passing velocity increases. The "stopper" (high stiffness material) in the damper is used to avoid the destruction of suspension, that is, if the suspension stroke is larger than maximum stroke, the suspension stiffness changes (increases) dramatically by the stopper. Furthermore, to verify the pure damper effect only without considering the effect of stoppers, inevitably lower velocity is adopted, and this setting does not have any issue while verifying the regulating performance of the controller during the transient.

The minimum and maximum values of each uncertain parameter are considered to generate the plant elements from the uncertain parameter, that is, 8 plant cases (grid size of 2). The responses of the proposed design are compared with the uncontrolled (passive) and SH control responses for the considered plant cases. Figure 7(A,B) compares the responses of the vertical and pitch angular displacements for the suspension system. The proposed design reduces the unwanted vibration in vertical and in angular motion very well for the eight plant cases. And, the responses due to the proposed design have smaller peak values as compared with the passive and SH control. The vertical and pitch angle acceleration, due to the proposed design, is better than the uncontrolled and SH over the time period as shown in Figure 7(C,D).

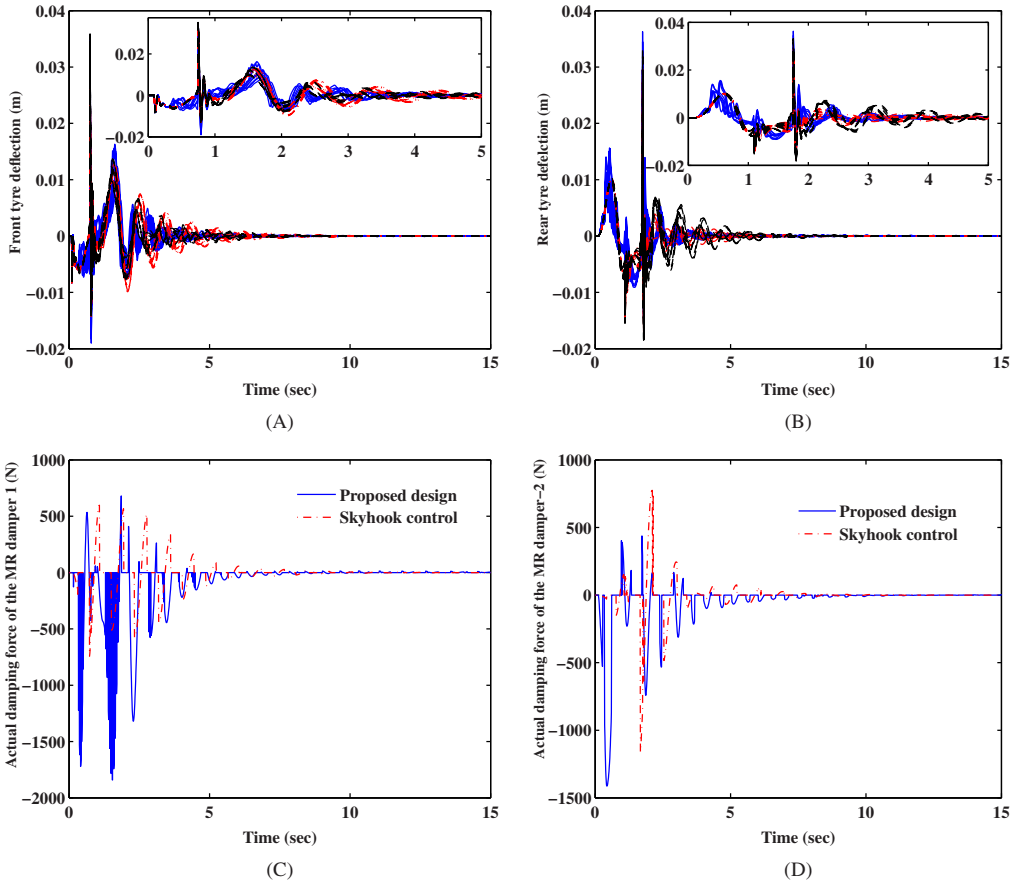

FIGURE 8 Comparison of the bump responses and damping forces (worst case); (A) front tyre deflection, (B) rear tyre deflection, (C) MR damper-1, and (D) MR damper-2. The dash-dot red line, dashed black line, and blue line denotes the passive control, Sky hook, and the proposed control, respectively. MR, magnetorheological [Colour figure can be viewed at wileyonlinelibrary.com]

TABLE 3 Comparison of the root mean square values (worst case) of displacement, acceleration, and tyre deflection under bump excitation

	Displacement		Acceleration		Tyre deflection	
Methods	**Vertical**	**Pitch**	**Vertical**	**Pitch**	**Front**	**Rear**
Passive	0.0202	0.0114	0.0081	0.0051	0.0029	0.0023
Skyhook	0.0193	0.0109	0.009	0.0045	0.0027	0.0029
Proposed design	**0.0085**	**0.006**	**0.0042**	**0.003**	**0.0021**	**0.0022**

Note: The bold values indicate the difference between the existing methods and the proposed design.

Figure 7(E,F) shows the suspension deflection plots for both front and rear tire under different methods. It is seen that the suspension deflection with the proposed design is less than the suspension limitations ($\leq$0.08 m^3) and comparable to the SH control. The passive suspension at the rear wheel hits the limits and creates the wear and tear to the suspension over the time period. Another important performance measure is the tire deflection (both front and rear). This is reduced substantially with the proposed design over the other control strategies as shown in Figure 8(A,B) for the considered uncertain case. The accelerations and the tire deflections are used to evaluate ride comfort and road holding of the vehicle (conflicting specification). Thus, the proposed design provides better ride comfort and road holding as compared with its counterpart. Figure 8(C,D) shows the actual damping force delivered by the MR dampers using the proposed controllers and the SH control. The root mean square (RMS) values of the displacements, accelerations, and tyre deflections reveals that the proposed design is better than the SH and passive methods as given in Table 3 for the worst plant case. For instance, the RMS values of the displacements and the accelerations are reduced by 50 % due to the proposed design as compared with the existing methods. Furthermore, we compare the output responses in-terms of performance measure such as integral absolute error (IAE) as given in Table 4 for the all the plant case. The IAE values (minimum and maximum) of the ride comfort and road holding are less in the proposed design over the SH and passive methods. Next, the sinusoidal disturbance is considered.

TABLE 4 Integral absolute error-based performance comparison under bump excitation

	Displacement(min,max)		Acceleration(min,max)		Tyre deflection(min,max)	
Methods	**Vertical**	**Pitch**	**Vertical**	**Pitch**	**Front**	**Rear**
Passive	[8.34,15.54]	[7.19,8.67]	[384.39,672.19]	[3.27,3.94]	[1.30,2.07]	[1.07,1.39]
Skyhook	[8.27,13.97]	[6.06,8.27]	[458.04,716.25]	[2.11,3.95]	[1.13,1.77]	[1.38,2.03]
Proposed design	**[4.73,6.77]**	**[3.86,4.98]**	**[283.90,399.55]**	**[2.13,3.21]**	**[1.21,1.37]**	**[1.06,1.29]**

Note: The bold values indicate the difference between the existing methods and the proposed design.

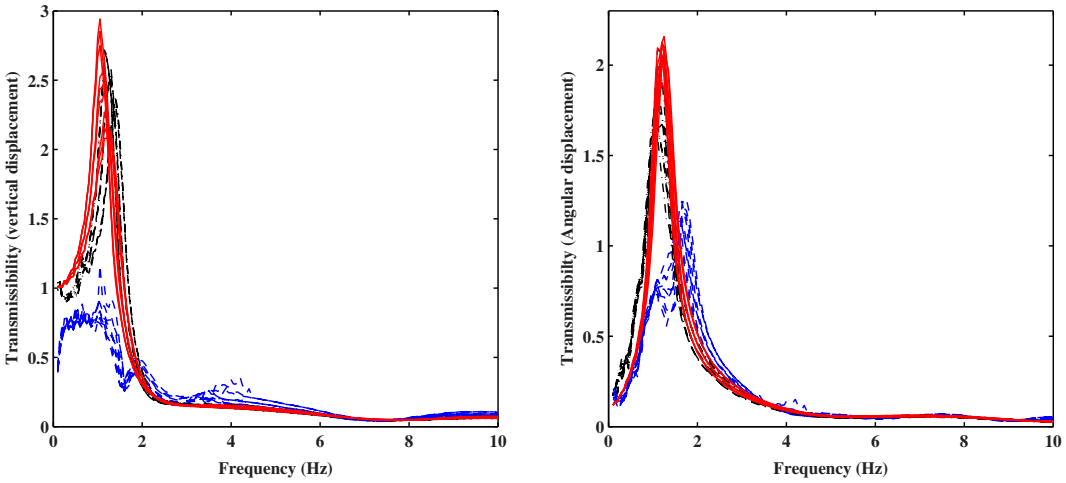

FIGURE 9 Transmissibility for displacement due to sinusoidal disturbance using different methods; (A) vertical motion and (B) pitch angle. Here, the solid red line, dashed black line, and dashed blue line represents the passive, Sky hook, and the proposed control, respectively [Colour figure can be viewed at wileyonlinelibrary.com]

5.2 | Sine disturbance

The second type of excitation is the sine function described by

$$z_{ri} = A_{mi} \sin(\omega t); \quad i = 1, 2. \tag{30}$$

Where, ω is the excitation frequency (0.1–10) Hz and A_{mi} (10 mm) denotes the amplitude. A comparison is made based on the transmissibility of the vertical and angular pitch displacement as shown in Figure 9. The RMS values (for all the eight plant cases) of input and output vertical displacements (and angular pitch displacement) are used to obtain the vertical displacement (and angular pitch displacement) transmissibility in the frequency domain. It is clearly shown, in Figure 9(A), that the transmissibility of the vertical displacement with the proposed controller has been substantially reduced in the neighborhood of the body resonance frequency (1–2 Hz) as compared with the SH control. Similarly, Figure 9(B) shows the transmissibility of the angular pitch displacement under different control strategies (eight plant case). It is seen that the transmissibility is reduced significantly around the body resonance under the proposed semiactive control.

5.3 | Random disturbance

The effectiveness of the proposed design is assessed by the random disturbance.[32,33] Random vibrations are typically specified as random process[32] with a given ground displacement PSD of

$$R_q(n) = R_q(n_0) \left(\frac{n}{n_0} \right)^{-W}, \tag{31}$$

where n is the spatial frequency and n_0 is the reference spatial frequency of $n_0 = 0.1(1/\text{m})$; $R_q(n_0)$ stands for the road roughness coefficient; W= 2 is the road roughness constant. Related to the time frequency f, we have $f = nV$ with V for the vehicle forward velocity. The PSD of ground displacement now becomes

$$R_q(f) = R_q(f_0)n_0^2\frac{V}{f^2}. \tag{32}$$

Then, the PSD of ground velocity is given by

$$R_{\dot{q}}(f) = (2\pi f)^2 R_q(f) = 4\pi^2 R_q(n_0)n_0^2 V. \tag{33}$$

Once the vehicle velocity is fixed, then the ground velocity can be seen as a white-noise signal. Finally, the PSD of body acceleration can be calculated[32] as

$$R_{\ddot{z}_s}(f) = |R(j\omega)|R_{\dot{q}}(f) = |R(j\omega)|4\pi^2 R_q(n_0)n_0^2 V. \tag{34}$$

Fix the vehicle velocity (V) as 30 km/h and we choose the random road roughness coefficient (ISO 2361) as $R_q(n_0) = 256 \times 10^{-6} m^3$ (Grade D - Poor).

Figure 10 compares the PSD of the vertical and the pitch angle acceleration for different controllers under the Grade-D road profile. It illustrates that the proposed design improves the ride comfort compared with its counterpart in spite of the poor road roughness, especially in the body resonance frequency range (1–2) Hz. Furthermore, it is seen that the PSD of the vertical and the pitch angle acceleration are reduced by more than 50% in the neighborhood of body resonance frequency range by implementing the proposed control strategy. As given in Table 5, the proposed controller yield smaller

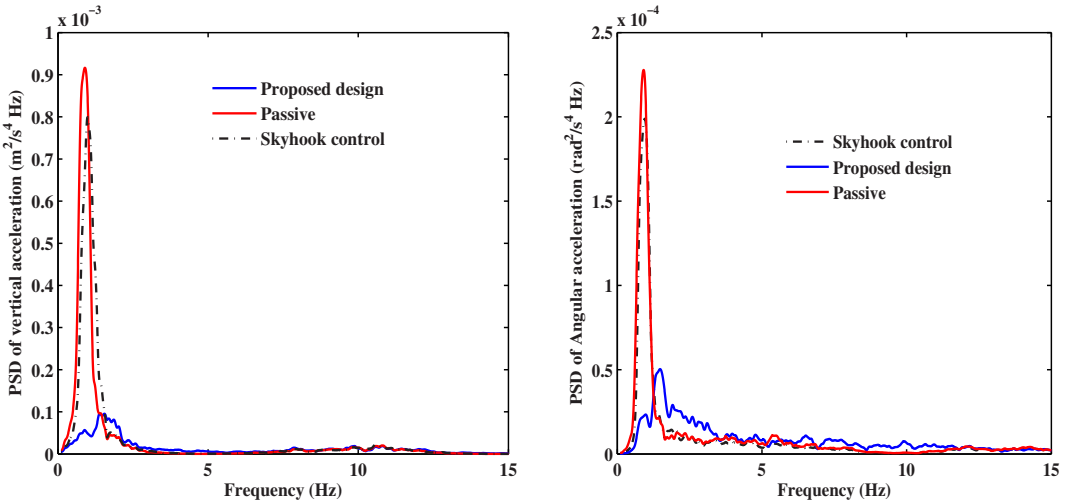

FIGURE 10 Comparison of power spectral density using different methods under Class D road profiles; (A) vertical acceleration and (B) pitch angle acceleration [Colour figure can be viewed at wileyonlinelibrary.com]

TABLE 5 Random excitation: Comparison of the root mean square value of accelerations

Methods	Acceleration	
	Vertical	Pitch
Passive	0.0254	0.0137
Skyhook	0.0322	0.0135
Proposed design	**0.0177**	**0.0125**

Note: The bold values indicate the difference between the existing methods and the proposed design.

RMS values for both vertical and pitch angular accelerations than the other methods. This shows the superiority of the proposed design and its practical implication.

6 | CONCLUSION

This article proposed the multivariable QFT design method to control the vertical and the pitch angle motion of a half-car vehicle model with semiactive MR damper suspension. The uncertainty originated from the payload variation and the crosscoupling behavior due to the off-diagonal elements posed a significant challenge from the controller design point of view. The crosscoupling effects between the vertical and pitch angle motion are minimized using the dynamic decoupler and the overall system becomes diagonally dominant system (noninteracting). On the other hand, the QFT design framework is used to design the robust controller for the decoupled system. The proposed design achieved the HF gain reduction (feedback cost) of around 10 and 15 dB over the sequential design for both equivalents SISO loop 1 and 2, respectively and implies that the proposed design is less sensitive to the noise under practical scenario. The proposed design reduces the vibration very well in the vertical and the pitch angle motions as compared with the passive and SH control under various road disturbances. For instance, the proposed method reduces the vertical and the pitch angle acceleration PSD by more than 50% in the neighborhood of body resonance frequency range under random road profile. The displacements and the accelerations are reduced substantially in the proposed design for the bump disturbance and its RMS values are atmost reduced by the 50%. These results imply that both ride comfort and steering stability of the half-car system can be improved significantly by adopting the proposed controller for the semiactive suspension system with MR dampers. As a future work, the extension of the proposed method to the full car suspension system could be an interesting one and the experimental validation of the proposed approach on a real car. Furthermore, it is interesting to explore an important global chassis control (bump disturbance) for automotive safety[34] and the steering problem[35] to control the overshoot for sideslip and yaw angles.

ACKNOWLEDGMENT

This work was supported by the National Research Foundation of Korea (NRF) grant funded by the Korea government (MEST) (No. 2017R1A2B3003026). This financial support is gratefully acknowledged.

CONFLICT OF INTEREST

The authors declare no potential conflict of interest.

ORCID

Seung-Bok Choi https://orcid.org/0000-0001-6262-2815

REFERENCES

1. Sun W, Pan H, Yu J, Gao H. Reliability control for uncertain half-car active suspension systems with possible actuator faults. *IET Control Theory Appl*. 2014;8(9):746-754.
2. Na J, Huang Y, Wu X, Gao G, Herrmann G, Jiang JZ. Active adaptive estimation and control for vehicle suspensions with prescribed performance. *IEEE Trans Control Syst Technol*. 2018;26(6):2063-2077.
3. Li H, Liu H, Hand S, Hilton C. Design of robust H_∞ controller for a half-vehicle active suspension system with input delay. *Int J Syst Sci*. 2013;44(4):626-640.
4. Shaer B, Kenné JP, Kaddissi C, Mintsa HA. Real time hybrid control of electrohydraulic active suspension. *Int J Robust Nonlinear Control*. 2017;27:4968-4991.
5. Fateh MM. Robust impedance control of a hydraulic suspension system. *Int J Robust Non Control*. 2010;20:858-872.
6. Choi SB, Han SS. H_∞ control of electro-rheological suspension system subjected to parameter uncertainties. *Mechatronics*. 2003;13(7):639-657.
7. Du H, Sze KY, Lam J. Semi-active H_∞ control of vehicle suspension with magneto-rheological dampers. *J Sound Vib*. 2005;283(3–5):981-996.
8. Savaresi SM, Spelta C. Mixed sky-hook and ADD: approaching the filtering limits of a semi-active suspension. *J Dyn Syst Meas Control*. 2007;129(4):382-392.
9. Karnopp DC, Corsby M, Harwood RA. Vibration control using semi-active force generators. *J Eng Ind*. 1974;96(2):619-626.
10. Choi SB, Lee SK, Park YP. A hysteresis model for the filed-dependent damping force of a magneto-rheological damper. *J Sound Vib*. 2001;254(2):375-383.

11. Poussot-Vassal C, Semane O, Dugard L, Gaspar P, Szabo Z, Bokor J. A new semi-active suspension control strategy through LPV technique. *Control Eng Pract*. 2008;16(12):1519-1534.
12. Karkoub MA, Zribi M. Active/semi-active suspension control using magnetorhological actuators. *Int J Syst Sci*. 2006;37(1):35-44.
13. Prabakar RS, Sujatha C, Narayanan S. Optimal semi-active preview control response of a half car vehicle model with magnetorheological damper. *J Sound Vib*. 2009;326(3–5):400-420.
14. Prabakar RS, Sujatha C, Narayanan S. Response of a half-car model with optimal magnetorheological damper parameters. *J Vib Control*. 2016;22(3):784-798.
15. Zhang H, Zhang N, Min F, Rakheja S, Su C, Wang E. Coupling mechanism and decoupled suspension control model of a half car. *Math Prob Eng*:1932107. 2016. https://doi.org/10.1155/2016/1932107.
16. Fleps-Dezasse M, Bünte T, Svaricek F, Brembeck J. LPV feedforward control of semi-active suspensions for improved roll stability. *Control Eng Pract*. 2018;78:1-11.
17. Liberzon A, Rubinstein D, Gutman PO. Active suspension for single wheel station of off-road track vehicle. *Int J Robust Nonlinear Control*. 2001;11(10):977-999.
18. Amani AM, Sedigh AK, Yazdanpanah MJ. A QFT approach to robust control of automobiles active suspension. Paper presented at: Proceedings of the 5th Asian Control Conference, Melbourne, Australia; 2004:604-610.
19. Zapateiro M, Pozo F, Karimi HR, Luo N. Semiactive control methodologies for suspension control with magnetorheological dampers. *IEEE/ASME Trans Mech*. 2012;17(2):370-380.
20. Jeyasenthil R, Choi SB. A novel semi-active control strategy based on the quantitative feedback theory for a vehicle suspension system with magneto-Rhelogical damper saturation. *Mechatronics*. 2018;54:36-51.
21. Jeyasenthil R, Choi SB. A novel semi-active control strategy based on the cascade quantitative feedback theory for a vehicle suspension system. *J Automot Eng*. 2019;233(7):1851-1863.
22. Savaresi SM, Poussot-Vassal C, Spelta C, Semane O, Dugard L. *Semiactive Suspension Control Design for Vehicles*. Oxford, UK: Butterworth-Heinemann; 2010.
23. Garcia-Sanz M. *Robust Control Engineering: Practical QFT Solutions*. Boca Raton, FL: CRC Press, Taylor & Francis; 2017.
24. Park I, Hong S, Sunwoo M. Robust air-to-fuel ratio and boost pressure controller design for the EGR and VGT systems using quantitative feedback theory. *IEEE Trans Control Syst Technol*. 2014;22(6):2218-2231.
25. Hariz MB, Bouani F. Robust fixed low order controller for uncertain decoupled MIMO systems. *J Dyn Syst Meas Control*. 2018;140(2):021001-021014.
26. Boje E. Non-diagonal controllers in MIMO quantitative feedback design. *Int J Robust Nonlinear Control*. 2002;12(4):303-320.
27. Garcia-Sanz M, Eguinoa I, Bennani S. Non-diagonal MIMO QFT controller design reformulation. *Int J Robust Nonlinear Control*. 2009;19(9):1036-1064.
28. Yaniv O. *Quantitative Feedback Design of Linear and Non-linear Control Systems*. The Netherlands: Kluwer Academic Publisher; 1999.
29. Choi SB, Li W, Yu M, Du W, Fu J, Do PX. State of the art of control schemes for smart systems featuring magneto-rheological materials. *Smart Mater Struct*. 2016;25:043001.
30. Liu Y, Zuo L. Mixed skyhook and power-driven-damper: a new low-jerk semi-active suspension control based on power flow analysis. *J Dyn Syst Meas Control*. 2016;138(8):081009:1-081009:10.
31. Skogestad S, Postlethwaite I. *Multivariable Feedback Control: Analysis and Design*. Hoboken, NJ: Wiley; 2005.
32. Sun W, Gao H, Kaynak O. Adaptive backstepping control for active suspension systems with hard constraints. *IEEE/ASME Trans Mech*. 2013;18(3):1072-1079.
33. Sun W, Li J, Zhao Y, Gao H. Vibration control for active seat suspension systems via dynamic output feedback with limited frequency characteristic. *Mechatronics*. 2011;21(1):250-260.
34. Fergani S, Menhour L, Semane O, Dugard L, Andréa-Novel BD. Integrated vehicle control through the coordination of longitudinal/lateral and vertical dynamics controllers: flatness and LPV/H_∞-based design. *Int J Robust Nonlinear Control*. 2017;27:4992-5007.
35. Barreras M, Villegas C, Garcia-Sanz M, Kalkkuhl J. Robust QFT tracking controller design for a car equipped with 4-wheel steer-by-wire. Paper presented at: Proceedings of the IEEE International Conference on Control Applications, Munich, Germany; 2006:1312-1317.

How to cite this article: Jeyasenthil R, Yoon DS, Choi S-B, Kim GW. Robust semiactive control of a half-car vehicle suspension system with magnetorheological dampers: Quantitative feedback theory approach with dynamic decoupler. *Int J Robust Nonlinear Control*. 2021;31:1418–1435. https://doi.org/10.1002/rnc.5355

APPENDIX

$$A=\begin{bmatrix} 0 & 0 & 0 & 0 & 1 & 0 & 0 & 0 & 0 & 0 \\ 0 & 0 & 0 & 0 & 0 & 1 & 0 & 0 & 0 & 0 \\ 0 & 0 & 0 & 0 & 0 & 0 & 1 & 0 & 0 & 0 \\ 0 & 0 & 0 & 0 & 0 & 0 & 0 & 1 & 0 & 0 \\ \frac{-(k_1+k_2)}{M} & \frac{-(k_1b_1-k_2b_2)}{M} & \frac{k_1}{M} & \frac{k_2}{M} & \frac{-(c_1+c_2)}{M} & \frac{-(c_1b_1-c_2b_2)}{M} & \frac{c_1}{M} & \frac{c_2}{M} & \frac{1}{M} & \frac{1}{M} \\ \frac{-(k_1b_1-k_2b_2)}{I} & \frac{-(k_1b_1^2+k_2b_2^2)}{I} & \frac{-k_1b_1}{I} & \frac{-k_2b_2}{I} & \frac{-(c_1b_1-c_2b_2)}{I} & \frac{-(c_1b_1^2+c_2b_2^2)}{I} & \frac{-c_1b_1}{I} & \frac{-c_2b_2}{I} & \frac{b_1}{I} & \frac{-b_2}{I} \\ \frac{k_1}{m_{t1}} & \frac{k_1b_1}{m_{t1}} & \frac{-(k_1+k_{t1})}{m_{t1}} & 0 & \frac{c_1}{m_{t1}} & \frac{c_1b_1}{m_{t1}} & \frac{-(c_1+c_{t1})}{m_{t1}} & 0 & \frac{-1}{m_{t1}} & 0 \\ \frac{k_2}{m_{t2}} & \frac{-k_2b_2}{m_{t2}} & 0 & \frac{-(k_2+k_{t2})}{m_{t2}} & \frac{c_2}{m_{t2}} & \frac{-c_2b_2}{m_{t2}} & 0 & \frac{-(c_2+c_{t2})}{m_{t2}} & 0 & \frac{-1}{m_{t2}} \\ 0 & 0 & 0 & 0 & 0 & 0 & 0 & 0 & \frac{-1}{\tau_1} & 0 \\ 0 & 0 & 0 & 0 & 0 & 0 & 0 & 0 & 0 & \frac{-1}{\tau_2} \end{bmatrix}, \tag{A1}$$

$$B=\begin{bmatrix} 0 & 0 & 0 & 0 & 0 & 0 & 0 & 0 & \frac{1}{\tau_1} & 0 \\ 0 & 0 & 0 & 0 & 0 & 0 & 0 & 0 & 0 & \frac{1}{\tau_2} \end{bmatrix}^T, \tag{A2}$$

$$L=\begin{bmatrix} 0 & 0 & 0 & 0 & 0 & 0 & 0 & 0 & \frac{k_{t1}}{m_{t1}} & 0 \\ 0 & 0 & 0 & 0 & 0 & 0 & 0 & 0 & 0 & \frac{k_{t2}}{m_{t2}} \end{bmatrix}^T, \tag{A3}$$

$$C=\begin{bmatrix} 1 & 0 & 0 & 0 & 0 & 0 & 0 & 0 & 0 & 0 \\ 0 & 1 & 0 & 0 & 0 & 0 & 0 & 0 & 0 & 0 \end{bmatrix}^T. \tag{A4}$$